

## Broadband enhancement of light harvesting in luminescent solar concentrator

Yun-Feng Xiao<sup>1</sup>, Chang-Ling Zou<sup>2</sup>, Yan Li<sup>1</sup>, Lixin Xiao<sup>1</sup>, Fang-Wen Sun<sup>2</sup>, and Qihuang Gong<sup>1</sup>

<sup>1</sup>State Key Lab for Mesoscopic Physics, School of Physics, Peking University, Beijing 100871, P. R. China and

<sup>2</sup>Key Lab of Quantum Information, University of Science and Technology of China, Hefei 230026, Anhui, P. R. China

(Dated: January 10, 2019)

Luminescent solar concentrator (LSC) can absorb large-area incident sunlight, then emit luminescence with high quantum efficiency, which finally be collected by a small photovoltaic (PV) system. The light-harvesting area of the PV system is much smaller than that of the LSC system, potentially improving the efficiency and reducing the cost of solar cells. Here, based on Fermi-golden rule, we present a theoretical description of the luminescent process in nanoscale LSCs where the conventional ray-optics model is no longer applicable. As an example calculated with this new model, we demonstrate that a slot waveguide consisting of a nanometer-sized low-index slot region sandwiched by two high-index regions provides a broadband enhancement of light harvesting by the luminescent centers in the slot region. This is because the slot waveguide can (1) greatly enhance the spontaneous emission due to the Purcell effect, (2) dramatically increase the effective absorption cross-section of luminescent centers, and (3) strongly improve the quantum efficiency of luminescent centers. It is found that about 80% solar photons can be ultimately converted to waveguide-coupled luminescent photons even for a low luminescent quantum efficiency of 0.5. This LSC is potential to construct a tandem structure which can absorb nearly full-spectrum solar photons, and also may be of special interest for building integrated nano-PV applications.

PACS numbers:

Obtaining high conversion efficiency at low cost is essential in photovoltaic (PV) system [1, 2]. In the past few years, many approaches involving nanostructures or nanostructured materials have been proposed to reduce cost and improve efficiency in both experiment [3–12] and theory [13–19]. On the other hand, concentrator PV systems in which large-area optical components collect direct sunlight and transfer the energy to small, high-efficiency PV cells have been suggested as a simple approach to lower the cost per peak Watt of PV systems for many decades [20]. To overcome the excess heat problem, chromatic aberrations and expensive maintaining in these imaging concentrators, luminescent solar concentrator (LSC) represents an alternative approach to lower the costs of PV systems [21–24]. LSCs generally consist of low-cost transparent sheets doped with luminescent species, such as dye molecules and quantum dots. Incident sunlight is highly absorbed by the luminescent centers and luminescence is emitted with high quantum efficiency, so that emitted photon is trapped in the sheet by the total internal reflection and travels to the edges where it can be collected by solar cells. The active material layer can be much thinner than the intrinsic absorption length of the material, thus dramatically reducing the amount of the solar cell material. Moreover, the conversion of the incident solar spectrum to narrow-band light in LSCs would greatly increase the efficiency of solar cells since some specific PV systems have near-unity response in a narrow-band spectrum.

One of the key parameters of LSCs is the coupling efficiency  $\beta$  which describes the ratio of luminescent photons coupled to waveguide modes for ultimate collection by PV systems on the waveguide edge. To model these LSC devices, thermodynamic and computational ray tracing approaches have been introduced, and both approaches represent a broad-scale, macroscopic model [24–28]. For example, conventional LSCs have a thickness much larger than the wavelength, so that the ray-optics model can be applied to estimate the collection efficiency of luminescence by the solar cell. However,

with LSC devices moving in the nanoscale, the ray-optics picture and some basic assumptions are no longer strictly applicable. In this paper, we propose a nanometer-sized slot waveguide as the main structure of LSC, and theoretically study the enhancement of spontaneous emission (described by the factor  $F_p$ ) of luminescent centers in this slot waveguide based on Fermi-golden rule. Remarkably, this great enhancement of spontaneous emission predicts not only an increased absorption cross-section of luminescent centers but also a very large waveguide coupling efficiency  $\beta$ . We demonstrate that such a slot waveguide LSC provides a broadband enhancement of light harvesting, and more than 80% re-emitted luminescent photons can be coupled into the slot waveguide modes for ultimate collecting by the solar cell located on the waveguide edge. This LSC may be of special interest for building integrated PV applications.

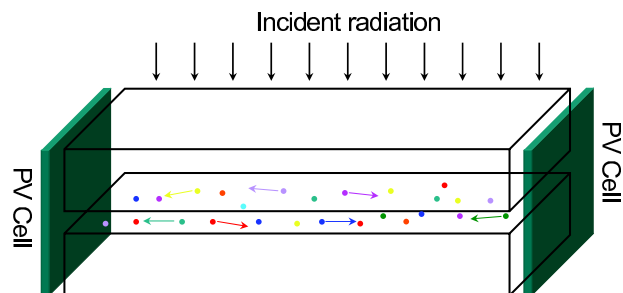


FIG. 1: Schematic illustration of a slot waveguide structured LSC. The slot waveguide consists of a nanometer-sized low-index slot region sandwiched by two high-index regions. Active medium such as dye molecules and quantum dots are located in the slot region. The PV system is on the edge of the slot waveguide and can collect the luminescent photons coupled in the slot waveguiding mode.

The basic structure of the proposed design is shown in Figure 1 and the cross-sectional geometry is depicted in Figure 2(b). The slot waveguide consists of a nanometer-sized low-

index slot region (with the permittivity  $\varepsilon_1 = n_1^2$ , here  $n_1$  is assumed 1.4) sandwiched by two high-index transparent layers (with the permittivity  $\varepsilon_2 = n_2^2$ , here  $n_2$  is assumed 3), and the PV systems are on the edge of the slot waveguide. Active medium such as dye molecules and quantum dots are doped in the slot region. The active medium absorbs the incident sunlight and re-emits the luminescence with a red-shifted wavelength. Different from the conventional waveguides, slot waveguide is able to guide and strongly confine light in a nanoscale low-index material. The basic principle of slot waveguide is based on the discontinuity of the electric field at a normal boundary between two materials [29]. When the electromagnetic wave propagates along the waveguide direction, the major component of the electric field of the quasi-transverse electric (TE) mode undergoes a discontinuity at the slot interfaces. According to boundary condition of Maxwell's equations, the amplitude of the electric field in the low-index slot is much larger than that in the high-index waveguides, and the ratio between them is  $\varepsilon_2/\varepsilon_1$ . With a full-vectorial finite element method (FEM), we can simulate the modes in the structure. As shown in Figure 2, the electric field of the quasi-TE mode is strongly concentrated in the slot region and it is normal to the interface, while the electric field of the quasi-transverse-magnetic (TM) mode distributes over the whole cross-sectional area and it is parallel to the interface. This unique characteristic makes the slot waveguide attractive for numerous applications, for instance, highly sensitive biosensors [30] and waveguide-based light source [31]. In this paper, also due to the large electric field intensity of the slot waveguide mode, the luminescent photons are expected to couple in the propagating slot mode, and finally be collected by the smaller high-efficiency PV systems. Due to the concentration effect at the LSC edges, the amount of the solar cell material reduces dramatically, and the cost of solar cell may decrease greatly with the help of the slot waveguide LSC.

To analyze this LSC system, we note that the conventional ray-optics model is not applicable because the thickness of the slot region is nanometer-sized. Thus, we derive a simple analytical formula from the Fermi-golden rule to obtain the spontaneous emission enhancement  $F_p$  and the waveguide coupling ratio  $\beta$ . In the weak-coupling regime, the spontaneous emission rate of a dipole can be calculated from

$$\gamma_{\text{WG}} = 2\pi |g(\vec{r})|^2 \rho(\omega), \quad (1)$$

where  $|g(\vec{r})|$  denotes the coupling strength between the dipole  $\vec{d}$  and the electromagnetic field  $\vec{E}$  at the dipole position  $\vec{r}$ .  $\rho(\omega)$  represents the density of states. If we assume that the dipole is oriented parallel to the electric field, the coupling strength is then given by

$$|g(\vec{r})| = \left| \vec{d} \cdot \vec{E}(\vec{r})/\hbar \right|, \quad (2)$$

with

$$\vec{E}(\vec{r}) = \sqrt{\frac{\hbar\omega}{2\varepsilon_0\varepsilon_1 A_{\text{eff}} l}} W(\vec{r}) \frac{\vec{E}(\vec{r})}{|\vec{E}(\vec{r})|}. \quad (3)$$

Here  $W(\vec{r})$  designates the normalized electromagnetic energy density distribution;  $A_{\text{eff}}$  defines the effective mode area as

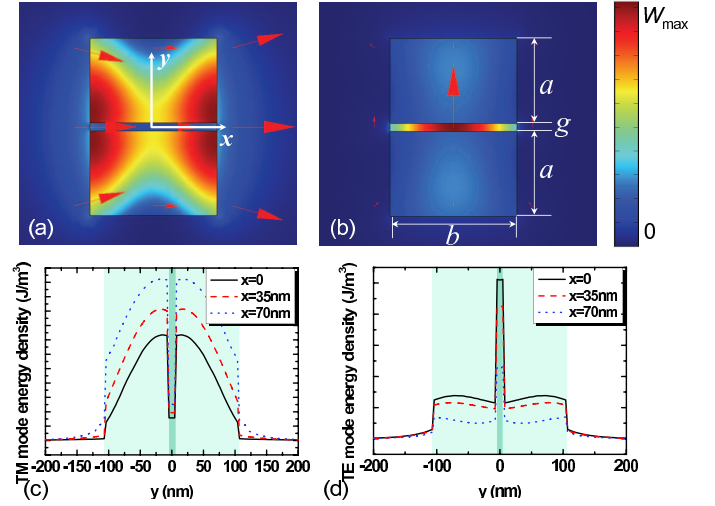


FIG. 2: (a), (b) False-color representations of electromagnetic energy density distributions  $W(\vec{r}) = \varepsilon_0 d(\varepsilon(\vec{r})\omega)/d\omega |\vec{E}(\vec{r})|^2 + \mu_0 |\vec{H}(\vec{r})|^2$  for quasi-TM and -TE modes, respectively, where the red arrows show the directions of the electric fields. The geometry of the slot waveguide is depicted in (b). (c), (d) Distributions of the normalized energy density  $W(\vec{r})$  along the  $y$  direction at several typical  $x$  positions for quasi-TE and -TM modes, respectively. Here,  $\lambda = 750$  nm;  $a = 100$  nm,  $b = 150$  nm and  $g = 10$  nm;  $n_1 = 1.4$ ,  $n_2 = 3$ .

$A_{\text{eff}} = \iiint_V \varepsilon_0 \varepsilon(\vec{r}) |\vec{E}(\vec{r})|^2 dV / \max[\varepsilon_0 \varepsilon(\vec{r}) |\vec{E}(\vec{r})|^2]$ , which plays the role analogous to the mode volume used in cavity QED;  $l$  is an arbitrary quantization length which can be canceled later. For a slot waveguide with a sufficiently small cross-sectional area, it only supports a single quasi-TE and a single quasi-TM mode. As mentioned before, the TE mode has the maximum electric field in the slot region. Thus, assuming a one-dimensional density of states, the density of states can be expressed as

$$\rho(\omega) = \frac{l}{\pi v_g(\omega)}, \quad (4)$$

where  $v_g = c/n_g$  is the group velocity of the slot waveguide mode with a group index  $n_g$ . Here,  $c$  is the light velocity in vacuum. Combining Equations (1)-(4), we can obtain the spontaneous emission rate of the dipole in the slot waveguide

$$\gamma_{\text{WG}} = 2\pi |\vec{d}|^2 W(\vec{r}) \frac{\omega}{2\hbar\varepsilon_0\varepsilon_1 A_{\text{eff}}} \frac{1}{\pi v_g(\omega)}. \quad (5)$$

With the spontaneous emission rate into free space  $\gamma_0 = d^2\omega^3/(3\pi\hbar\varepsilon_0 c^3)$ , the emission enhancement also known as Purcell effect, is thus expressed as

$$F_p \equiv \frac{\gamma_{\text{WG}}}{\gamma_0} = \frac{3}{4\pi} \frac{c}{v_g(\omega)} \frac{(\lambda_0/n_1)^2}{A_{\text{eff}}} W(\vec{r}). \quad (6)$$

Clearly, if the effective mode area  $A_{\text{eff}}$  of the slot waveguide mode is squeezed significantly below  $\lambda_0^2$ , the light-matter interaction can be dramatically enhanced, thus leading to an enhanced  $F_p$ . In addition, the group velocity in the slot waveguiding mode is reduced, which can furthermore increase the

local density of states and also contribute to the increase of  $F_p$ . Once the emission enhancement is given, the waveguide coupling efficiency  $\beta$  describing the ratio of the emission coupled to the slot waveguiding mode, can be calculated as

$$\beta = \frac{F_p}{F_p + n_1}. \quad (7)$$

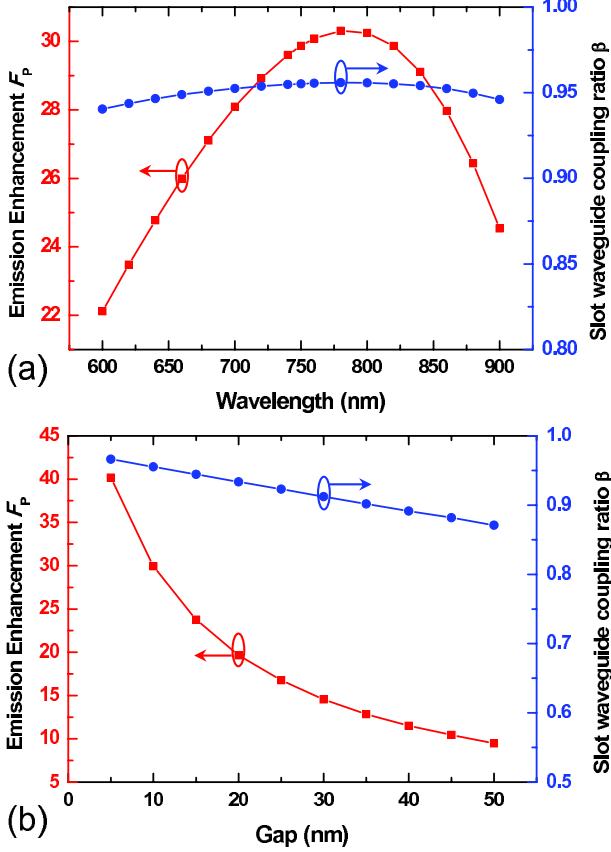


FIG. 3: (a) Spontaneous emission enhancement ( $F_p$ ) and waveguide coupling efficiency ( $\beta$ ) depending on the working wavelength for slot waveguides with  $g = 10$  nm. (b)  $F_p$  and  $\beta$  depending on the slot width (gap)  $g$  with  $\lambda = 750$  nm. In all cases,  $a = 100$  nm,  $b = 150$  nm.

Equations (6) and (7) represent the main physical parameters of the proposed LSC. To numerically evaluate the emission enhancement and the waveguide coupling efficiency, we still resort to the FEM simulation, as it can provide not only the mode distribution ( $f(\vec{r})$ ,  $A_{\text{eff}}$ ) but also the group velocity  $v_g(\omega)$  for a given geometry and working wavelength. Figure 3 shows the calculated  $F_p$  and  $\beta$  as a function of free-space wavelength  $\lambda_0$  when a dipole is placed in the center of the cross-section of the slot waveguide. We find two points. (i)  $F_p$  first increases and then decreases with the emission wavelength from 600 to 900 nm. This phenomenon is because that the effective mode area  $A_{\text{eff}}/\lambda_0^2$  first decreases and then increases. (ii)  $F_p$  exceeds 22 over the whole calculation range. This strong enhancement of the spontaneous emission takes advantage of nonresonance (large bandwidth), which benefits from the subwavelength mode area (as small as

$0.02 (\lambda_0/n_1)^2$ ) and the reduced group velocity (with the group index  $n_g \sim 3.2 - 3.5$ ) provided by the slot waveguide. Remarkably, this broadband enhancement character overcomes the narrow bandwidth limit of a microresonator-based emission enhancement. As a result, most of the spontaneous emission can efficiently couple to the slot waveguide mode, and  $\beta$  is as high as 0.95 over a broad wavelength range. This range of 600 to 900 nm can exactly cover the whole emission spectrum for a specific type of dye molecules, for instance, platinum tetraphenyltetrabenzoporphyrin [Pt(TPBP)] [32].

It is not difficult to know that the enhancement of spontaneous emission depends on the geometry of the slot waveguide, for example, the slot width. Figure 4 shows the calculated enhancement factor  $F_p$  as a function of the slot width  $g$ . The factor  $F_p$  monotonically increases with reducing the slot width. For example,  $F_p$  increases from 10 to 40 when  $g$  decreases from 50 to 5 nm. The underlying physics is that both the effective mode area and the group velocity are strongly reduced by decreasing the slot width. For instance,  $A_{\text{eff}}$  and  $n_g$  are  $0.0185 \mu\text{m}^2$  and 2.56 at  $g = 50$  nm,  $0.00643 \mu\text{m}^2$  and 3.77 at  $g = 5$  nm. Thus, in this slot width range, the waveguide coupling efficiency  $\beta$  changes from 0.87 to 0.96.

In the analysis above, we have assumed that the dipole is oriented parallel to the electric field of the quasi-TE mode. In an actual case, the orientation of a dipole may be isotropically distributed over any direction. In general, the quasi-TE mode has a much stronger electric field concentration in the slot region than the quasi-TM mode. As a result, the dipole oscillating in the  $y$  direction (coupled to the quasi-TE mode) exhibits a much larger emission enhancement than the dipole oscillating in the  $x$  direction (coupled to the quasi-TM mode). In addition, the spontaneous emission enhancement of the dipole oscillating in the  $z$  direction is even smaller because both the modes are quasi-transverse. The isotropically averaged emission enhancement factor  $\bar{F}_p$  can be calculated by

$$\bar{F}_p = \frac{F_{p,x} + F_{p,y} + F_{p,z}}{3}, \quad (8)$$

where  $F_{p,i=x,y,z}$  denotes the spontaneous emission enhancement when the dipole oscillates in the  $i$  direction. With  $\bar{F}_p$ , the isotropically averaged waveguide coupling efficiency  $\bar{\beta}$  is thus obtained as

$$\bar{\beta} = \frac{\bar{F}_p}{\bar{F}_p + n_1}. \quad (9)$$

Figure 4(a) and 4(b) show  $\bar{F}_p$  and  $\bar{\beta}$ , respectively, depending on the emission wavelength for three different slot widths  $g = 10, 20, 30$  nm. From Figure 4(a), on one hand, due to enhanced dipole-field coupling,  $\bar{F}_p$  increases as the slot width decreases. On the other hand,  $\bar{F}_p$  still keeps high over the whole calculation range from 600 to 900 nm. Thus, even if dipoles oscillate in random directions, most emission of the dipoles will couple into the waveguide modes. For instance, as demonstrated in Figure 4(b), the averaged waveguide coupling efficiency  $\bar{\beta}$  is high above 0.85 over a broad wavelength range in the case of  $g = 10$  nm.

It should also be noted that only spontaneous emission is modified by the concentrated slot mode, while the intrinsic

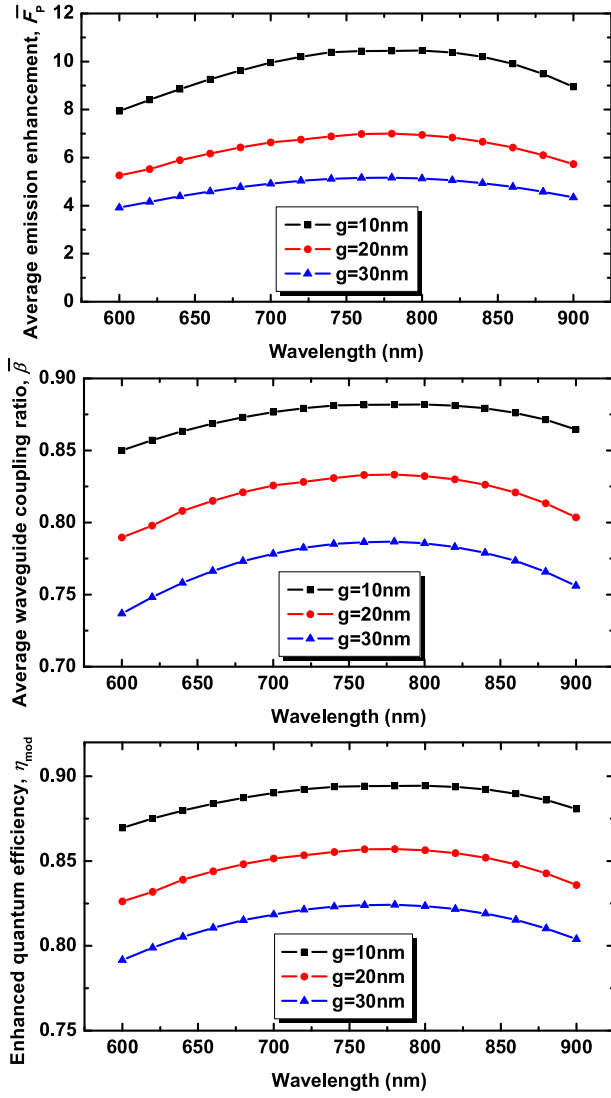


FIG. 4: (a), (b) Average spontaneous emission enhancement ( $\bar{F}_p$ ) and average waveguide coupling efficiency ( $\bar{\beta}$ ) depending on the working wavelength for slot waveguides, respectively. (c) The enhanced quantum efficiency  $\eta$  as a function of wavelength with initial quantum efficiency  $\eta_0 = 0.5$ . In all cases,  $a = 100$  nm,  $b = 150$  nm.

nonradiative decay of the dipole related to the quantum efficiency ( $\eta_0$ ) keeps unchanged. The discussion above has assumed a unit quantum efficiency ( $\eta_0 = 1$ ). For a finite quantum efficiency, however, we find that the spontaneous emission enhancement can actually improve the quantum efficiency. In the slot waveguide, the modified quantum efficiency  $\eta_{\text{mod}}$  describing the ratio of the radiation, can be calculated by

$$\eta_{\text{mod}} = \frac{\eta_0(1 + \bar{F}_p/n_1)}{(1 - \eta_0) + \eta_0(1 + \bar{F}_p/n_1)}. \quad (10)$$

As demonstrated in Figure 4(c), for an initial  $\eta_0 = 0.5$ , the modified efficiency  $\eta_{\text{mod}}$  exceeds 0.85 over a broad wavelength range in the case of  $g = 10$  nm.

We turn to analyze the total photon conversion efficiency with this LSC. Besides the isotropically averaged waveguide

coupling efficiency  $\bar{\beta}$  and the modified quantum efficiency  $\eta_{\text{mod}}$ , the total efficiency  $\eta_{\text{total}}$  should also include the solar photon absorption efficiency  $\eta_{\text{abs}}$  by the active medium, the transportation efficiency  $\eta_{\text{tran}}$  from emitters to the PV systems, and the quantum efficiency  $\eta_{\text{PV}}$  of the PV systems. Thus, we have

$$\eta_{\text{total}} = \eta_{\text{abs}}\eta_{\text{mod}}\bar{\beta}\eta_{\text{tran}}\eta_{\text{PV}}. \quad (11)$$

In the following we will explain how the slot waveguide play significant roles in obtaining a high  $\eta_{\text{total}}$ . First,  $\eta_{\text{abs}}$  depends on the intrinsic property of the active medium, such as the absorption cross-section and the absorption spectrum. However, the absorption ability of single emitters is expected to improve due to the enhanced emission with a high  $\bar{F}_p$  in the slot waveguide. Each luminescent center can absorb more solar photons within a given time because its absorption-emission round time is strongly shortened. In other words, the absorption length of the slot region is efficiently increased, namely, light trapping. Second, from Figure 4, it is not difficult to find that the slot waveguide can improve both  $\eta_{\text{mod}}$  and  $\bar{\beta}$  over a broad wavelength range, which can be further improved by aligning the dipoles of luminescent centers parallel to the electric field of quasi-TE modes [33]. Third, the luminescent photons should be transported to the LSC edges where the PV systems can absorb these photons and convert them to photoelectrons. In this process, the photon transportation efficiency  $\eta_{\text{tran}}$  can be high because the slot provides good propagating modes along  $z$  direction with small radiation loss. Nevertheless,  $\eta_{\text{tran}}$  may be degraded by the re-absorption phenomenon of the active medium. Fortunately, the re-absorption can be suppressed by choosing luminescent centers whose absorption and emission spectra have a small overlap due to a large Stokes shift, or using luminophores with unitary internal quantum efficiency which effectively closes the nonradiative decay channel [34]. In addition, a high photon transportation efficiency  $\eta_{\text{tran}}$  is beneficial for achieving a high concentration as the waveguide can be long in this case. Lastly, since the PV systems indirectly absorb solar photons, the thickness of PV systems can be very small and it provides better collection of photo-generated charge carriers. Thus,  $\eta_{\text{PV}}$  can be easily optimized.

If we assume that the solar photon absorption efficiency by luminescent centers  $\eta_{\text{abs}}$  is 0.9, the transportation efficiency from emitters to the PV systems  $\eta_{\text{tran}}$  is 0.9, the quantum efficiency of the PV systems  $\eta_{\text{PV}}$  is 0.9, and the slot width  $g = 10$  nm, the initial quantum efficiency of luminescent centers  $\eta_0 = 0.5$ , we can obtain  $\bar{\beta} > 0.85$ ,  $\eta_{\text{mod}} > 0.85$ , and  $\eta_{\text{total}} > 50\%$ . In other words, more than 50% solar photons can be converted to photoelectrons. To obtain the highest power efficiencies, on one hand, the absorption band can be broadened by mixing dyes and quantum dots with different size. On the other hand, it is also potential to construct tandem LSCs which can absorb more solar photons in a broad band. Incident solar photons are first absorbed by a LSC employing a short-wavelength active medium, such as a specific dye. Photons with longer wavelengths are transmitted through the first LSC and then absorbed by the second LSC employing a long-wavelength active medium, as shown in Figure 5. Moreover, the active layer of PV systems on the edge can also

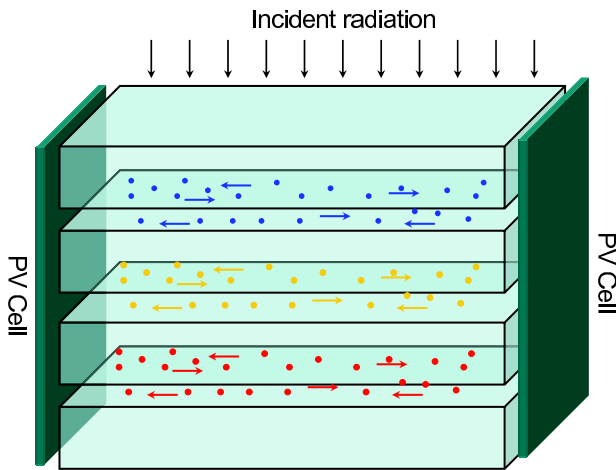


FIG. 5: Schematic illustration of a tandem slot waveguide structured LSC. From top to bottom, the slot waveguides absorb solar photons with increasing wavelengths

be designed into the slot structure which strongly traps the luminescence from our LSC [13]. This further improves solar cell efficiency, because thinner active layer provides better collection of photo-generated charge carriers. Finally, to fabricate such a LSC structure, a nanoprinting technique can be utilized.

In summary, we present a theoretical description of nanoscale LSC where the conventional ray-optics model is no longer applicable. Based on Fermi-golden rule, we evaluate the spontaneous emission enhancement  $F_p$  and the waveguide coupling efficiency  $\beta$  in a slot waveguide consisting of a nanometer-sized low-index slot region sandwiched by two high-index regions. It is found that the slot waveguide provides a broadband enhancement of light harvesting by the luminescence centers in the slot region. In spite of a low luminescence quantum efficiency  $\eta_0 \sim 0.5$ , approximately 90% solar photons re-emitt as luminescent photons, and more than 80% luminescence can be coupled into the waveguide modes for ultimate absorption by the solar cell located on the waveguide edge. This LSC concept holds a great potential to construct a tandem structure thus absorbing nearly full-spectrum solar photons, and is of special interest for building integrated nano-PV applications.

The authors acknowledge financial support from the National Natural Science Foundation of China under Grant No. 10821062 and 11004003, the National Basic Research Program of China under Grant Nos. 2006CB921601, 2007CB307001 and 2009CB930504. Yun-Feng Xiao was also supported by the Research Fund for the Doctoral Program of Higher Education (No.20090001120004) and the Scientific Research Foundation for the Returned Overseas Chinese Scholars.

- 
- [1] M. Gratzel, Photoelectrochemical cells, *Nature* 414 (2001) 338-344.
- [2] N.S. Lewis, Toward cost-effective solar energy use, *Science* 315 (2007) 798-801.
- [3] W.U. Huynh, J.J. Dittmer, A.P. Alivisatos, Hybrid nanorod-polymer solar cells, *Science* 295 (2002) 2425-2427.
- [4] M. Law, L.E. Greene, J.C. Johnson, R. Saykally, P. Yang, Nanowire dye-sensitized solar cells, *Nature Material* 4 (2005) 455-459.
- [5] J.B. Baxter, E.S. Aydil, Nanowire-based dye-sensitized solar cells, *Appl. Phys. Lett.* 86 (2005) 053114.
- [6] B.Z. Tian, et al., Coaxial silicon nanowires as solar cells and nanoelectronic power sources, *Nature* 449 (2007) 885-890.
- [7] H.A. Atwater, A. Polman, Plasmonics for improved photovoltaic devices, *Nature Material* 9 (2010) 205-213.
- [8] D.H. Ko, J.R. Tumbleston, L. Zhang, S. Williams, J. M. DeSimone, R. Lopez, E.T. Samulski, Photonic Crystal Geometry for Organic Solar Cells, *Nano Lett.* 9 (2009) 2742-2746.
- [9] J. Zhu, et al., Optical Absorption Enhancement in Amorphous Silicon Nanowire and Nanocone Arrays, *Nano Lett.* 9 (2008) 279-282.
- [10] E. Garnett, P.D. Yang, Light Trapping in Silicon Nanowire Solar Cells, *Nano Lett.* 10 (2010) 1082-1087.
- [11] M.D. Kelzenberg, et al., Enhanced absorption and carrier collection in Si wire arrays for photovoltaic applications, *Nature Material* 9 (2010) 239-244.
- [12] J.G. Mutitu, et al., Thin film solar cell design based on photonic crystal and diffractive grating structures, *Opt. Express* 16 (2008) 15238-15248.
- [13] Z. Yu, A. Raman, S. Fan, Fundamental limit of nanophotonic light-trapping in solar cells, arXiv:1004.2902.
- [14] A. Aubry, et al., Plasmonic light-harvesting devices over the whole visible spectrum, *Nano Lett.* 10 (2010) 2574-2579.
- [15] Y. Zhang, L.W. Wang, A. Mascarenhas, "Quantum Coaxial Cables" for Solar Energy Harvesting, *Nano Lett.* 7 (2007) 1264-1269.
- [16] B.M. Kayes, H.A. Atwater, N.S. Lewis, Comparison of the device physics principles of planar and radial p-n junction nanorod solar cells, *J. Appl. Phys.* 97 (2005) 114302.
- [17] L.Y. Cao, et al., Semiconductor Nanowire Optical Antenna Solar Absorbers, *Nano Lett.* 10 (2010) 439-445.
- [18] W. Wang, S. Wu, K. Reinhardt, Y. Lu, S. Chen, Broadband light absorption enhancement in thin-film silicon solar cells, *Nano Lett.* 10 (2010) 2012-2018.
- [19] P.F. Scudo, L. Abbondanza, R. Fusco, L. Caccianotti, Spectral converters and luminescent solar concentrators, *Solar Energy Materials and Solar Cells* 94 (2010) 1241-1246.
- [20] J.H. Karp, E.J. Tremblay, J.E. Ford, Planar micro-optic solar concentrator, *Opt. Express* 18 (2010) 1122-1133.
- [21] W.H. Weber, J. Lambe, Luminescent greenhouse collector for solar radiation, *Appl. Opt.* 15 (1976) 2299-2300.
- [22] J.S. Batchelder, A.H. Zewail, T. Cole, Luminescent solar concentrators 2: Experimental and theoretical analysis of their possible efficiencies. *Appl. Opt.* 1981, 20, 3733-3754.
- [23] A. Goetzberger, W. Greubel, Solar energy conversion with fluorescent collectors, *Appl. Phys.* 14 (1977) 123-139.
- [24] M.J. Currie, J.K. Mapel, T.D. Heidel, S. Goffri, M.A. Baldo, High-Efficiency Organic Solar Concentrators for Photovoltaics, *Science* 321 (2008) 226-228.
- [25] A.J. Chatten, K.W.J. Barnham, B.F. Buxton, N.J. Ekins-Daukes, M.A. Malik, Quantum Dot Solar Concentrators, *Semiconductors* 38 (2004) 609-617.

- [26] A.A. Earp, G.B. Smith, P.D. Swift, J. Franklin, Maximising the light output of a Luminescent Solar Concentrator, *Sol. Energy* 76 (2004) 655-667.
- [27] M. Carrascosa, S. Unamuno, F. Agullo-Lopez, Monte Carlo simulation of the performance of PMMA luminescent solar collectors, *Appl. Opt.* 22 (1983) 3236-3241.
- [28] U. Rau, F. Einsele, G.C. Glaeser, Efficiency limits of photovoltaic fluorescent collectors, *Appl. Phys. Lett.* 87 (2003) 171101.
- [29] V.R. Almeida, Q.F. Xu, C.A. Barrios, M. Lipson, Guiding and confining light in void nanostructure, *Opt. Lett.* 29 (2004) 1209-1211.
- [30] C.A. Barrios, et al., Slot-waveguide biochemical sensor, *Opt. Lett.* 32 (2007) 3080-3082.
- [31] Y.C. Jun, R.M. Briggs, H.A. Atwater, M.L. Brongersma, Broadband enhancement of light emission in silicon slot waveguides, *Opt. Express* 17 (2009) 7479-7490.
- [32] M.E. Thompson, The evolution of Organometallic complexes in Organic light-emitting devices, *Mater. Res. Bull.* 32 (2007) 694.
- [33] R.W. MacQueen, Y.Y. Cheng, R.G.C.R. Clady, T.W. Schmidt, Towards an aligned luminophore solar concentrator, *Opt. Express* 18 (2010) A161-A166.
- [34] T. Saraidarov, V. Levchenko, A. Grabowska, P. Borowicz, R. Reisfeld, Non-self-absorbing materials for Luminescent Solar Concentrators (LSC), *Chem. Phys. Lett.* 492 (2010) 60-62.